JOURNAL OF Applied Polymer SCIENCE

# Hydrogenated Petroleum Resin Effect on the Crystallization of Isotactic Polypropylene

**Jian Kang, Jingping Li, Shaohua Chen, Shipeng Zhu, Huilin Li, Ya Cao, Feng Yang, Ming Xiang**
State Key Laboratory of Polymer Materials Engineering, Polymer Research Institute of Sichuan University, Chengdu 610065, People's Republic of China
Correspondence to: F. Yang (E-mail: yf_fengyang@126.com) or M. Xiang (E-mail: xiangming45@hotmail.com)

**ABSTRACT:** The influence of the hydrogenated petroleum resin P125 on the crystallization behavior, crystallization kinetics, and optical properties of polypropylene (PP) were investigated. The results of differential scanning calorimetry, successive self-nucleation, and annealing fractionation demonstrated that P125 reduced the interaction between the PP molecules, decreased the crystallization, prevented PP from forming thick lamellae, and encouraged the formation of thin lamellae. The isothermal crystallization kinetics, self-nucleation isothermal crystallization kinetics, and polarized optical microscopy observations showed that P125 slightly decreased the nucleation rate, significantly decreased the crystal growth rate, generally reduced the overall crystallization rate, and effectively deceased the crystallite sizes of PP. The optical properties studies showed that P125 effectively decreased the haze and increased the surface glossiness and yellowness index of PP. © 2013 Wiley Periodicals, Inc. J. Appl. Polym. Sci. 130: 25–38, 2013

**KEYWORDS:** crystallization; morphology; polyolefins

Received 11 July 2012; accepted 4 October 2012; published online 8 March 2013
**DOI: 10.1002/app.38699**

## INTRODUCTION

Petroleum resin comes from blends of unsaturated monomers obtained as volatile byproducts in the cracking of natural gas, gas oil, and so on. The unsaturated monomers consist of mono-olefins, diolefins, cyclic olefins, and vinyl derivatives of aromatic hydrocarbons. A hydrogenate procedure is often used to obtain hydrogenated petroleum resin (HPR). HPRs are commonly characterized by their color, iodine number, specific gravity, solution viscosity, softening point, and aniline point. They have water resistance, wide compatibility with polyolefins, chemical neutrality, good electrical properties, and well-balanced adhesive characteristics.

Because of the advantages mentioned previously, HPRs are widely added to polypropylene (PP) to modify its structure, morphology and properties, especially in film production. The consumption of HPRs in PP applications is large. Researchers have mainly paid attention to the phase behavior crystallization, morphology, and properties of PP blended with low-molecular resins similar to HPRs, for instance, hydrogenated oligocyclopentadiene.[1–4] They have also investigated the crystallization, morphology, and properties of PP/HPR mixtures;[5–7] great progress in investigating the phase structure, overall crystallization behavior, and structure has been made. However, in previous studies, the detailed influence of HPRs on the crystallization behavior and crystallization kinetics (e.g., the separated primary nucleation kinetics and crystal growth kinetics) is still not clear yet; this is of great importance in determining the multiscale morphology and properties of PP.[8,9] Currently, the application of HPRs on PP is still in its experiential stage, and this has restrained the scientific application of HPRs and the property design of PP products.

In classical crystallization theories, the temperature dependence of the overall crystallization rate ($G_o$) can be expressed by two exponential factors: the nucleation term and the crystal growth (molecular transport) term.[10–13] For many semicrystalline polymers, including PP, it has been found that these two factors have different crystallization peak temperature ($T_c$) dependence behaviors and thereby display a bell-shaped temperature dependence of $G_o$, with a maximum $G_o$ at a maximum $T_c$.[10–13] At low supercoolings (the high-crystallization region), the thermal movement of the molecular chains is intense, and the crystal growth term is dominant; At high supercoolings (the low-$T_c$ region), the molecular chain diffusion becomes very difficult, and the nucleation term is dominant. As the temperature decreases and even approaches the glass-transition temperature ($T_g$), the crystallization nearly ceases. On the other hand, it is necessary for the melt to be supercooled to form stable nuclei; therefore, the higher the supercooling degree is, the more favorable the thermodynamic conditions will be for nuclei formation.

HPRs have a softening point above which the resin is a liquid; below the softening point, HPRs are solid. Interestingly, the softening point of HPRs is usually within the $T_c$ region of PP. Different temperature regions might lead to different phase behaviors of HPRs and may further influence the crystallization behavior of PP.

Unsatisfactory optical properties restrict the industrial application of PP, although the resin usually has superior mechanical properties. Therefore, it is important to explore methods for improving the optical properties, that is, to reduce the turbidity, to increase the surface glossiness, and so on. One method for modifying the optical properties is the introduction of additives, such as nucleating agents, that will vary the crystallization behavior of PP.[14] However, the detailed influence of HPRs on the optical properties of PP and their relation to the crystallization behavior are still unknown.

It would be helpful to design the morphology and properties of PP if the influence of HPR on the crystallization behavior, crystallization kinetics, and optical properties could be studied. The aim of this research was to study the influence of HPR on the crystallization behavior, crystallization kinetics, and optical properties of PP and their relationships in detail.

## EXPERIMENTAL

### Materials

The PP resin used was resin from a biaxially oriented PP film (trade name T38F), which was produced by Lanzhou Petro-Chemical Corp., China; it had a melt flow index of 3.0 g/10 min (2.16 kg), a number-average molecular weight of 120,000, a weight-average molecular weight of 370,000, and a molecular weight dispersity of 3.08.

HPR (trade name P125, produced by Idemilsu Petro-Chemica's (Japan) Polymerization and Hydrogenation Technologies, with a number-average molecular weight of 880 and a softening point of 125°C) was used.

The PP pellets and P125 were mixed at weight ratios of 100: 5, 100: 10, and 100: 15, respectively, and were then mixed in a HAAKE PolyLab instrument, German. The processing conditions were as follows: a temperature of 200°C, a rotation rate of 30 rpm, and a mixing time of 10 min.

### Characterization

**Differential Scanning Calorimetry (DSC).** All of the calorimetric experiments were carried out on a Mettler Toledo DSC1 differential scanning calorimeter Switzerland under a nitrogen atmosphere (50 mL/min). Calibration for the temperature scale was performed with indium as a standard to ensure reliability in the data obtained. To ensure the homogeneity of the samples and good contact between the sample and the pan, the virgin polymer was molded at 200°C and 10 MPa for 5 min into sheets with a uniform thickness of about 300 $\mu$m. Then, 5-mg round samples were punched out of the sheets. The HPR was amorphous and did not crystalize. Therefore, in the calculation of the degree of crystallinity ($X_c$) of the blends, the amount of P125 was subtracted. The experimental error of the measured $T_c$ and melting peak temperature ($T_m$) was ±0.1°C.

**Successive Self-Nucleation and Annealing (SSA) Fractionation.** The complete thermal treatment of SSA fractionation included the following steps:

1. Erasing the thermal history by heating the sample to 200°C and holding for 5 min.
2. Cooling the sample at 20°C/min to 30°C and holding for 2 min
3. Heating the sample at 20°C/min from 30°C to a partial melting temperature denoted as $T_s$.
4. Keeping the sample at $T_s$ for 15 min.
5. Running a DSC cooling scan at 20°C/min from $T_s$ to 30°C, where the effects of the thermal treatment were reflected on the crystallization of the sample.
6. Repeating steps 3–5 at increasingly lower $T_s$ values, which were varied from 167 to 139°C at 4°C intervals for a total of eight self-nucleation/annealing steps.
7. Finally, heating the sample at 10°C/min from 30 to 200°C to obtain a multiple melting endotherm.

The first $T_s$ to be used in step 4 was carefully chosen as 167°C, which was the lowest temperature within domain II (or the self-nucleation domain, defined by Fillon and coworkers[15–17]) of the PP resin studied in this article.

**Isothermal Crystallization.** The isothermal crystallization kinetics were studied according to the following procedures: (1) the samples were heated from 30 to 200°C at 10°C/min under a nitrogen atmosphere and kept there for 5 min to erase any previous thermal history, (b) the samples were quickly cooled down to a desired $T_c$ at 50°C/min, and (3) the samples were isothermally retained for the period of time necessary to complete the crystallization.

**Self-Nucleation Isothermal Crystallization Kinetics (Scheme 1).** The self-nucleation isothermal crystallization kinetics were measured according to the following procedures: First, the self-nucleating behavior of the samples was measured according to Fillon and coworkers,[15–17] and the temperature region for the self-nucleation domain (domain II) was determined. Then, samples were held at 200°C under a nitrogen atmosphere for 5 min to destroy any residual nuclei. After that, the samples were cooled to 30°C at 10°C/min and held there for 2 min to create a "standard" thermal history; they were then heated again to the self-nucleating temperature (the lowest temperature within domain II was desired, and in this study, the self-nucleating temperature was 167°C) and kept there for 5 min. Then, the sample was rapidly cooled to a predetermined $T_c$ and held there for a period of time, which was long enough to allow complete isothermal crystallization. Finally, the sample was heated to 200°C at a rate of 10°C/min.

**Polarized Optical Microscopy (POM).** The superstructural morphology of the samples was studied with a Zeiss MC-80 (German) polarized light microscope. Thin melt samples were prepared between microscope coverslips. They were melted at 200°C for 5 min and then cooled to room temperature at a cooling rate of 5°C/min.

**Wide-Angle X-Ray Diffraction (WAXD).** The samples were molded at 200°C and 10 MPa for 5 min into sheets of a uniform thickness of about 100 $\mu$m for WAXD measurement. All

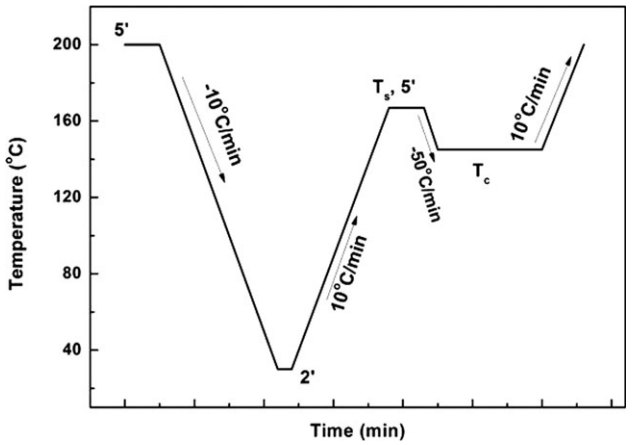


**Scheme 1.** Thermal treatment protocol of the self-nucleation isothermal crystallization kinetics.

of the WAXD experiments were performed with a DX-1000 diffractometer, Haoyuan Instrument Corp., China. The wavelength of Cu Kα was $\lambda = 0.154$ nm, and the spectra were recorded in the 2θ range of 5–35° at a scanning rate of 2°/min with a scanning step of 0.02°. The crystallite size ($L$) of each plane of samples was determined from XRD with the Debye–Scherrer equation:[18]

$$L = 0.9\lambda/\beta\cos\theta$$

where $\lambda$ is the X-ray wavelength of radiation used, θ is the Bragg angle, and $\beta$ is the full width of the diffraction line at the half-maximum intensity (rad).

The content of the $\beta$-crystal form was determined according to standard procedures described in the literature[19] with the following relation:

$$k_\beta = \frac{H_\beta(300)}{H_\beta(300) + H_\alpha(110) + H_\alpha(040) + H_\alpha(130)}$$

where $k_\beta$ denotes the relative content of the $\beta$-crystal form (WAXD); $H_\alpha(110)$, $H_\alpha(040)$, and $H_\alpha(130)$ are the intensities of the strongest peaks of the $\alpha$ form attributed to the (110), (040), and (130) planes of the monoclinic cell, respectively; and $H_\beta(300)$ is the intensity of the strongest (300) diffraction peak of the trigonal $\beta$ form.

**Optical Properties.** Films with a thickness about 100 $\mu$m were prepared by compression-molding at 200°C and 10 MPa for 5 min, and the optical parameters, the yellowness index (YI), surface glossiness, and turbidity ($\tau$), were measured.

***YI.*.** Polymer discoloration of the samples were monitored by changes in YI.[20,21] The samples were measured with a Hunter-Lab (USA) colorimeter according to ASTM D 1925.

***τ.*** $\tau$ was defined by the following equation:[14]

$$\tau = (1/d)\ln(I_0/I_t) \quad (1)$$

where $I_o$ and $I_t$ are the intensities of the incident and transmitted lights, respectively, and $d$ is the thickness of the sample.

***Surface glossiness.*.** The surface glossiness of the samples was measured by a glossmeter (model 520, Zhongcun optical electronic instrument Corp., China), according to GB/T 8807-1988. The details were reported in Ref. 22.

## RESULTS AND DISCUSSION

### DSC Cooling and Melting Behavior

The DSC cooling and subsequent heating curves at a rate of 10°C/min are shown in Figure 1. The melting and cooling parameters obtained are listed in Table I, where $T_{m\text{endset}} - T_{m\text{onset}}$ (where $T_{m\text{endset}}$ and $T_{m\text{onset}}$ are the endset and onset melting temperatures, respectively) is an evaluation standard of the $T_m$ range of the sample. The larger $T_{m\text{endset}} - T_{m\text{onset}}$ is, the wider the melting temperature range of the sample is.

Figure 1 and Table I show that after the addition of P125, $T_c$ and the onset and endset crystallization temperatures ($T_{c\text{onset}}$ and $T_{c\text{endset}}$, respectively) on the cooling curves all decreased gradually. Meanwhile, $T_{m\text{onset}}$ and $T_{m\text{endset}}$, $T_m$ on the melting curves, and $X_c$ decreased gradually; this indicated that P125 restrained the formation of thick lamellae and reduced the crystallizability of PP. On the other hand, the melting range

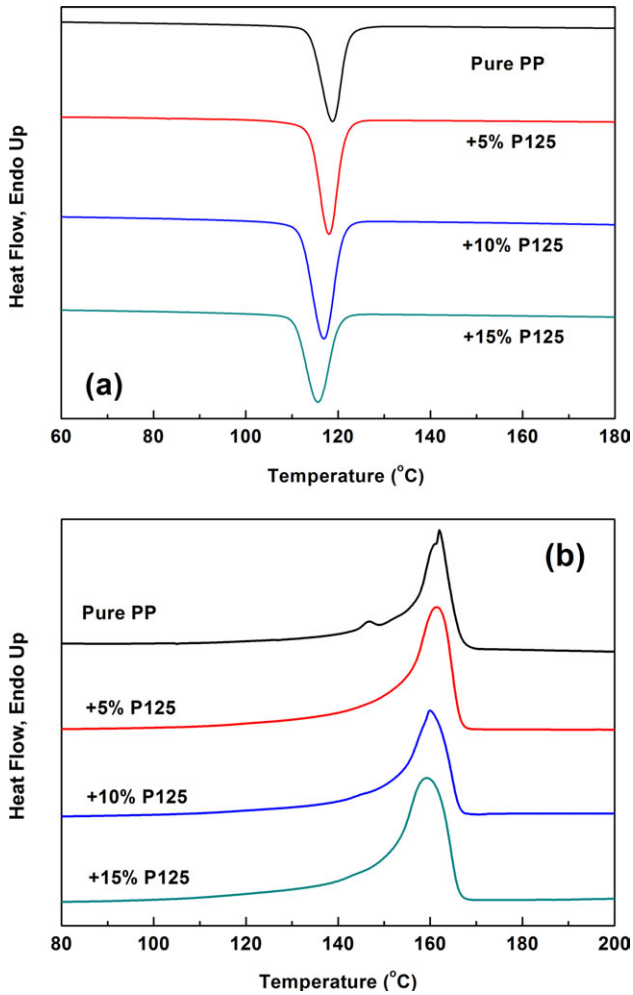


**Figure 1.** (a) Cooling curves and (b) subsequent heating curves of PP with P125 at a rate of 10°C/min. [Color figure can be viewed in the online issue, which is available at wileyonlinelibrary.com.]

**Table I.** Crystallization and Melting Parameters of PP with P125

| Sample | Cooling scan | | | Heating scan | | | | |
|---|---|---|---|---|---|---|---|---|
| | $T_{conset}$ | $T_c$ | $T_{cendset}$ | $T_{monset}$ | $T_m$ | $T_{mendset}$ | $X_c$ | $T_{mendset} - T_{monset}$ |
| Pure PP | 122.6 | 118.8 | 114.6 | 155.3 | 162.0 | 166.4 | 47.4 | 11.1 |
| +5% P125 | 122.8 | 118.1 | 114.5 | 153.3 | 161.3 | 166.5 | 46.6 | 13.2 |
| +10% P125 | 121.2 | 116.9 | 112.5 | 151.6 | 160.0 | 166.3 | 43.4 | 14.7 |
| +15% P125 | 120.2 | 115.5 | 110.5 | 150.0 | 159.4 | 166.1 | 42.2 | 16.1 |

($T_{mendset}$–$T_{monset}$) increased gradually as the amount of P125 increased; this indicated that the distribution of lamellar thickness became broader.

### WAXD Characterization

The obtained WAXD profiles of the samples are shown in Figure 2. The crystallite parameters, *d*-spacing, *L*, relative degree of crystallinity (*X*), and $k_\beta$, are listed in Tables II and III. Note that in the calculation of $X_c$ of the samples, the amount of P125 was subtracted.

As shown in Tables II and III, for the pure PP, the emergence of the peak at $2\theta = 16°$, characteristic of the $\beta$ (300) plane, indicated the formation of $\beta$ crystals. $k_\beta$ was 16.1%. However, after the addition of P125, the peak at $2\theta = 16°$ disappeared; this may have indicated that P125 prevented PP from forming $\beta$ crystals. On the other hand, as the amount of P125 increased, nearly all of the *d*-spacing of the crystal planes of PP increased, and *L* and *X* decreased. This indicated that the addition of P125 made the crystal particles more loosely packed and decreased *L* of PP.

### SSA Fractionation

SSA is widely used in tacticity studies of polyolefins[23–37] and can also be used to study the influence of additives on the crystallization behavior of polyolefins.[38–40] In this study, SSA fractionation was used to quantitatively study the influence of P125 on the crystallization behavior of PP.

### SSA Curves and the Lamellar Thickness Distribution

The SSA final melting curves of the samples are shown in Figure 3. To benefit discussion, the peak located at the highest temperature is denoted as peak 1, and the following main peak located at a high temperature is denoted as peak 2.

The lamellar thickness was estimated from the SSA curve with the Thomson–Gibbs equation,[41] according to which the SSA curves were converted into lamellar thickness distribution curves, as shown in Figure 4:

$$T_m = T_m^0\left(1 - \frac{2\sigma}{\Delta H_0 L}\right) \tag{2}$$

where $T_m^0$ is the equilibrium melting temperature and is equal to 460 K[42,43], $\Delta H_0$ is the equilibrium melting enthalpy per unit volume and is equal to $184 \times 10^6$ J/m$^3$, $\sigma$ is the surface energy and is equal to 0.0496 J/m$^2$, and *L* is the lamellar thickness.[44]

As shown in Figures 3 and 4, when 5% P125 was added, the $T_m$ located at the highest temperature (peak 1) disappeared. As the amount of P125 increased, the SSA melting curve gradually shifted toward the lower temperature region; this indicated that the thickness of the formed lamellae decreased. Meanwhile, $X_c$ decreased gradually, and this indicated that a lesser amount of crystal formed after the same SSA protocol.

To further the analysis, the statistical parameters describing the lamellar thickness, the arithmetic average lamellar thickness ($L_n$), weighted average lamellar thickness ($L_w$), and broadness index (*I*), were calculated with the following equations.[45]

$$I = \frac{L_w}{L_n} \tag{3}$$

$$L_n = \frac{n_1L_1 + n_2L_2 + n_3L_3 + n_4L_4 + , \ldots, + n_jL_j}{n_1 + n_2 + n_3 + n_4 + , \ldots, + n_j} = \sum f_iL_i \tag{4}$$

$$L_n = \frac{n_1L_1^2 + n_2L_2^2 + n_3L_3^2 + n_4L_4^2 + , \ldots, + n_jL_j^2}{n_1L_1 + n_2L_2 + n_3L_3 + n_4L_4 + , \ldots, + n_jL_j} = \frac{\sum f_iL_i^2}{\sum f_iL_i} \tag{5}$$

where $n_i$ is the normalized peak area and $L_i$ is the lamellar thickness for each fraction. The quantitative results obtained are listed in Table IV.

Table IV shows that as the amount of P125 increased, $L_n$, $L_w$, and *I* decreased gradually. This indicated that P125 decreased

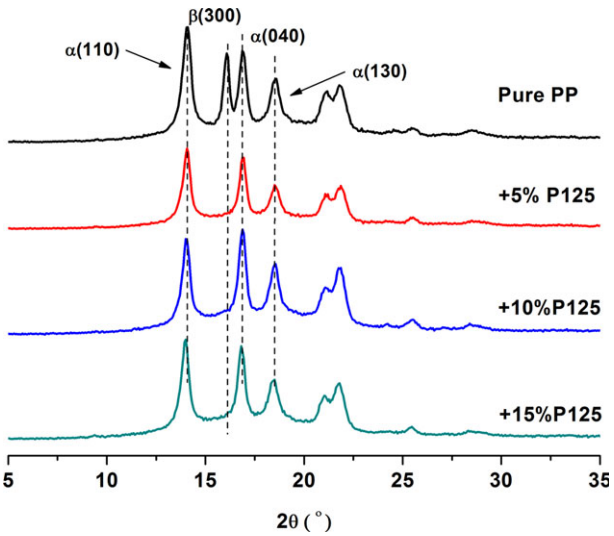


**Figure 2.** WAXD profiles of PP with different contents of P125. [Color figure can be viewed in the online issue, which is available at wileyonlinelibrary.com.]

**Table II.** Crystallite Parameters of the PP Samples with P125 Obtained from WAXD

| Parameter | Sample | α(110) | β(300) | α(040) | α(130) | α(111) | α(041) |
|---|---|---|---|---|---|---|---|
| *d*-spacing (A) | Pure PP | 6.2907 | 5.5219 | 5.2343 | 4.7843 | 4.2012 | 4.0607 |
| | +5% P125 | 6.2914 | — | 5.2402 | 4.7870 | 4.2050 | 4.0622 |
| | +10% P125 | 6.3061 | — | 5.2464 | 4.7982 | 4.2120 | 4.0704 |
| | +15% P125 | 6.3180 | — | 5.2544 | 4.8054 | 4.2254 | 4.0797 |
| *L* (nm) | Pure PP | 18.9 | 25.1 | 22.4 | 14.9 | 14.3 | 12.7 |
| | +5% P125 | 18.5 | — | 21.1 | 14.6 | 13.6 | 12.2 |
| | +10% P125 | 17.9 | — | 20.1 | 14.0 | 12.8 | 11.9 |
| | +15% P125 | 17.1 | — | 19.7 | 13.4 | 12.5 | 11.4 |

the crystallizability of PP and restrained the formation of thick lamellae.

### Influence of P125 on the Contents of the Lamellae with Different Thicknesses

Figure 5 shows the curves of accumulated crystallinity as a function of the melting temperature of the samples. To quantitatively study the variation of the relative crystallinity of the formed lamellae with different thicknesses after the addition of P125, a melting range of 120–180°C on the SSA curves was divided into six temperature regions, and the relative crystallinity in each temperature range was calculated, as shown in Table V.

Figure 5 and Table V show that as the amount of P125 increased, the relative crystallinity in the high-temperature ranges (>160°C) decreased gradually. This suggested that lamellae with lower thicknesses formed. Meanwhile, the relative crystallinity in the low-temperature ranges under 160°C increased gradually; this indicated that a greater amount of thin lamellae formed. These results illustrate that P125 restrained the formation of thick lamellae and encouraged the formation of thin lamellae for PP. Finally, the values of the relative degree of crystallinity at crystallization time $t$ ($X_t$) in the temperature range below 160°C increased gradually as the amount of P125 increased.

Because of the structural similarity of PP and P125, the blend in this study was miscible in the melt state;[6] therefore, the presence of P125 molecules might have modified the motion of PP macromolecules in the melt and reduced the interaction between PP macromolecules. Finally, the formation of thick lamellae for PP was restrained, and more thin lamellae formed.

### Isothermal Crystallization Kinetics

P125 possesses softening behavior and a softening point at 125°C, which is located just within the $T_c$ of PP. To fully investigate the influence of P125 on the crystallization kinetics, the isothermal crystallization kinetics were studied in a large temperature range, which covered the softening point of P125, from 121 to 130°C.

The curves of $X_t$ as a function of $t$ and the corresponding exothermic DSC curves at these temperatures are presented in Figure 6. $X_t$ here is a relative value and can be defined as follows:

$$X_t = \int_0^t (dH_c/dt)dt \Big/ \int_0^\infty (dH_c/dt)dt \qquad (6)$$

where $dH_c$ denotes the measured enthalpy of crystallization during the isothermal time interval $dt$. The limits $t$ and $\infty$ denote the elapsed time during the course of crystallization and at the end of the crystallization process, respectively.

The half-crystallization time ($t_{o1/2}$), which is defined as the half-period (i.e., 50% crystallization) from the onset of crystallization to the end of crystallization, can be a direct measure of the crystallization rate. The reciprocal of $t_{o1/2}$, represented by $G_{o1/2}$ [eq. (7)], can also be used as a parameter characterizing the overall crystallization rate of the samples.

$$G_{o1/2} = 1/t_{o1/2} \qquad (7)$$

**Table III.** $X$ and $k_\beta$ Values of the Samples

| Sample | $k_\beta$ (%) | $X$ (%) |
|---|---|---|
| Pure PP | 16.1 | 50.6 |
| +5% P125 | 0.0 | 49.6 |
| +10% P125 | 0.0 | 46.3 |
| +15% P125 | 0.0 | 42.2 |

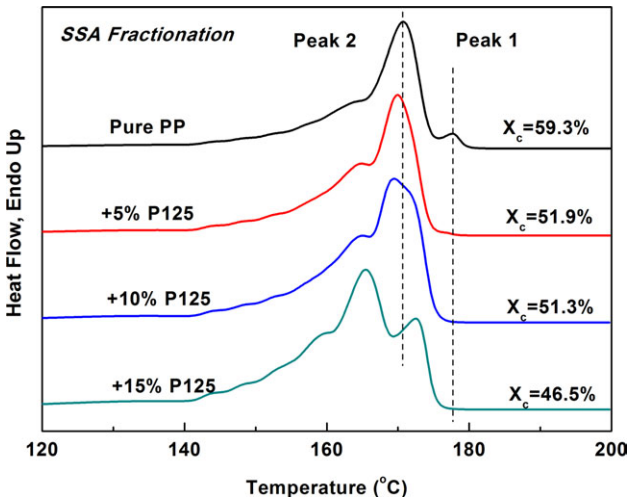


**Figure 3.** SSA fractionation curves of the PP samples. The peak located at the highest temperature is denoted as peak 1, and the following main peak located at a high temperature is denoted as peak 2. [Color figure can be viewed in the online issue, which is available at wileyonlinelibrary.com.]

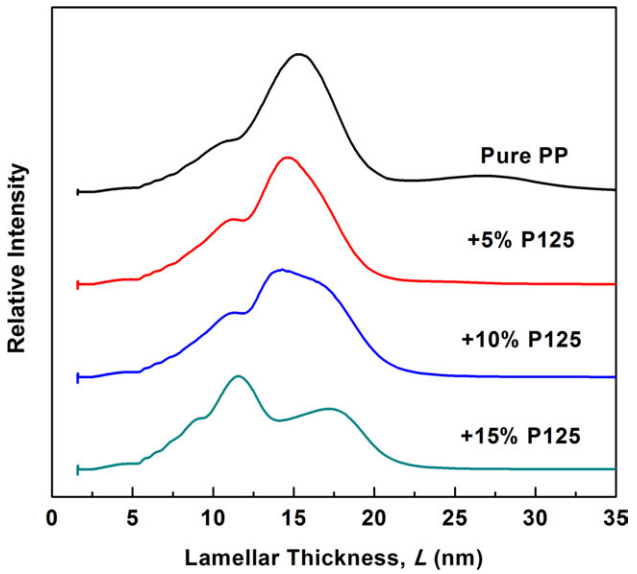


**Figure 4.** Lamellar thickness distribution curves of the PP samples. [Color figure can be viewed in the online issue, which is available at wileyonlinelibrary.com.]

The Avrami equation, a semiempirical expression, is widely applied to indirectly characterize the dimensionality of growth in polymer crystallization; it is used to analyze the isothermal crystallization kinetics of samples. The logarithmic form of the Avrami model is expressed as shown in eq. (8):[46]

$$\ln[-\ln(1 - X_t)] = \ln K_n + n\ln t \tag{8}$$

where $n$ is the Avrami exponent and $K_n$ is the crystallization rate parameter involving both the primary nucleation and growth rate of crystals. By fitting the experimental data to eq. (8), we obtained the values of $n$ and $K_n$. $n$ is broadly used to describe dimensionality as the regions from lower than 2, 2 to 3, and 3 to 4, which correspond to one-, two-, and three-dimensional growth, respectively.[47] Because some of the curves of $\log[-\ln(1 - X_t)]$ versus $\log t$ are not always linear in the whole range, a linear fitting is applied to the linear parts of the curves in the log $t$ range below 0.4. The variation of $t_{o1/2}$, $G_{o1/2}$, and $K_n$ as a function of the isothermal $T_c$ are shown in Figure 7. The Avrami plots of $\log[-\ln(1 - X_t)]$ versus $\log t$ for the isothermal crystallization process of the samples are shown in Figure 8, and the values of $n$ are listed in Table VI.

As shown in Figure 7(a–c), the parameters describing the overall crystallization rate ($G_{o1/2}$ and $K_n$) decreased gradually as the amount of P125 increased; this indicated that P125 decreased the overall crystallization behavior of PP.

**Table IV.** Average Lamellar Thickness Parameters of the Samples

| Sample name | $L_w$ | $L_n$ | $I = L_w/L_n$ |
|---|---|---|---|
| Pure PP | 14.7 | 13.2 | 1.11 |
| +5% P125 | 14.3 | 13.1 | 1.09 |
| +10% P125 | 14.2 | 13.0 | 1.09 |
| +15% P125 | 13.3 | 12.3 | 1.08 |

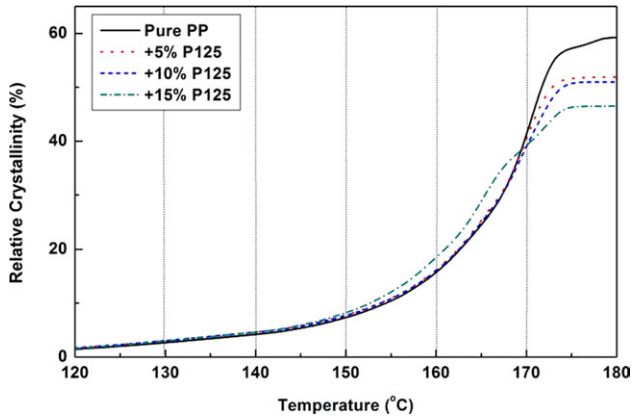


**Figure 5.** Relative area percentage as a function of the melting temperature calculated from the SSA curves of the samples. [Color figure can be viewed in the online issue, which is available at wileyonlinelibrary.com.]

Meanwhile, Figure 8 shows that after the addition of P125, for pure PP, the curves of $\log[-\ln(1 - X_t)]$ versus $\log t$ were almost linear over the whole range. However, for samples with P125, many curves contained two linear parts; this indicated that there appeared to be two different stages during isothermal crystallization. To study the crystallization behavior in the early stage, a linear fitting was applied on the left linar part of the curves, and $n$ was obtained, as shown in Table VI. For pure PP, the majority of the $n$ values were larger than 2; this denoted two-dimensional growth. However, for samples with P125, at low $T_c$ (<125°C), the $n$ values were lower than 2; this indicated one-dimensional growth. At high $T_c$ (125–130°C), the $n$ values were higher than 2; this suggested that the crystallization dimensionality changed to two-dimensional growth. This change might have been due to the different phase states of P125 when $T_c$ was below or above the softening point, 125°C.

To further the study, the $t_{o1/2}$ value at $T_c$ = 121°C [$t_{o1/2(121°C)}$] of each sample was taken as a reference, and all of the $t_{o1/2}$ values at $T_c$ = 121–130°C were normalized. Their variation as a function of $T_c$ is shown in Figure 9.

Figure 9 shows that for pure PP, $t_{o1/2(130°C)}$ was 4.95 times the value of $t_{o1/2(121°C)}$. However, for the PP sample with 15% P125, this value was 7.52. This suggested that the greater the amount of P125 was, the higher the rate of increase of $t_{o1/2}$ was; namely, the greater the decrease rate of $G_o$ was.

The influence of the softening point of P125 on the crystallization behavior of PP could be explained as follows. When the temperature was lower than the softening point, P125 was solid, and the interaction between P125 and PP molecules was slight. Therefore, the restraint on the crystallization rate was slight. When the temperature was higher than the softening point, P125 was in the molten state. Because of the molecular structural similarity between P125 and PP, the compatibility between the two components was good. Therefore, the molten P125 might have decreased the interaction of the PP molecules and significantly decrease $G_o$. The higher the content of P125 was,

**Table V.** $X_c$ Value of Each Temperature Region on the SSA Curves of the Samples

| Sample | $X_c$ (%) | <130°C | 130–150°C | 150–160°C | 160–170°C | 170–180°C | >180°C |
|---|---|---|---|---|---|---|---|
| Pure PP | 59.3 | 3.05 | 4.61 | 7.94 | 24.97 | 18.43 | 0.30 |
| +5% P125 | 51.9 | 3.09 | 4.66 | 8.37 | 23.55 | 12.17 | 0.00 |
| +10% P125 | 51.3 | 3.17 | 4.72 | 9.05 | 23.27 | 11.15 | 0.00 |
| +15% P125 | 46.5 | 3.22 | 5.15 | 9.37 | 21.53 | 7.23 | 0.00 |

the higher the increase rate of $t_{o1/2}$ was when $T_c$ increased from 121 to 130°C.

### Self-Nucleation Isothermal Crystallization

In the isothermal crystallization study, both primary nucleation and crystal growth made a contribution to the overall crystallization kinetics of PP. To separate the contribution of these two factors, the self-nucleation isothermal crystallization kinetics[48] were studied. It was assumed that during the process, the sample was fully nucleated. Then, the sample was rapidly cooled down and isothermally crystallized at a desired temperature ($T_{cSN}$). In this way, the subsequent isothermal crystallization could be used to study the crystal growth kinetics. The value of $T_{cSN}$ was settled on the basis of experimental consideration. For pure PP, $T_{cSN}$ = 138–142°C; for samples with P125, because of the low crystal growth rate ($G$), the $T_{cSN}$ was chosen as 126–130°C.

The curves of $X_t$ as a function of $t$ at $T_{cSN}$ are shown in Figure 10. The corresponding exothermic DSC curves at these temperatures are also presented in the inset of Figure 10.

The half-crystal growth time ($t_{c1/2}$), which is a direct measure of $G$, in the self-nucleation isothermal crystallization measurement. $G_{c1/2}$ (the reciprocal of $t_{c1/2}$) could also be used as a parameter to characterize the crystal growth rate $G$. The higher $G_{c1/2}$ is, the faster $G$ was.

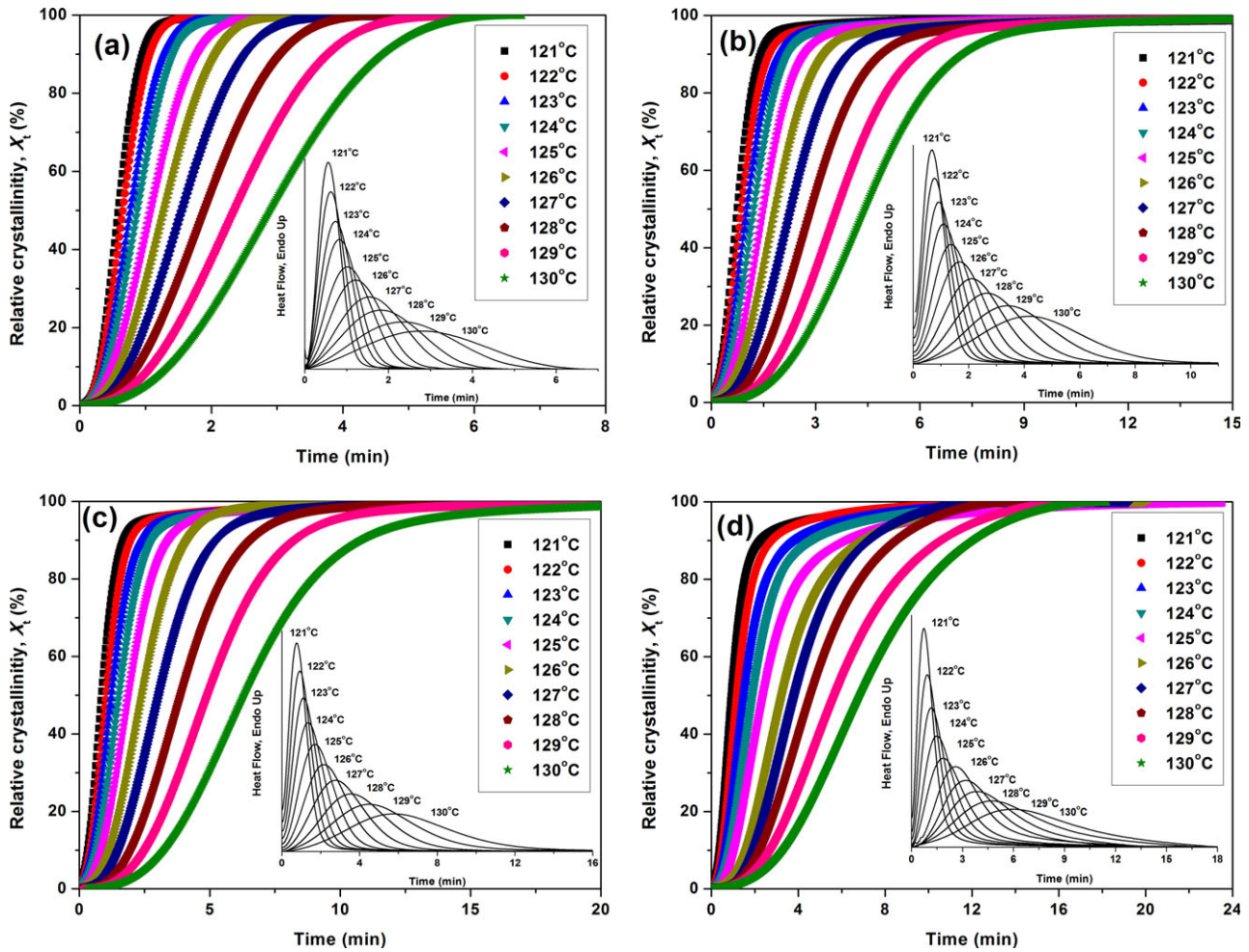


**Figure 6.** Plots of the relative crystallinity versus $t$ for (a) pure PP, (b) 5% P125, (c) 10% P125, and (d) 15% P125 isothermally crystallized at 121–130°C. The inset gives the corresponding exothermic DSC curves at these temperatures. [Color figure can be viewed in the online issue, which is available at wileyonlinelibrary.com.]

Applied Polymer SCIENCE

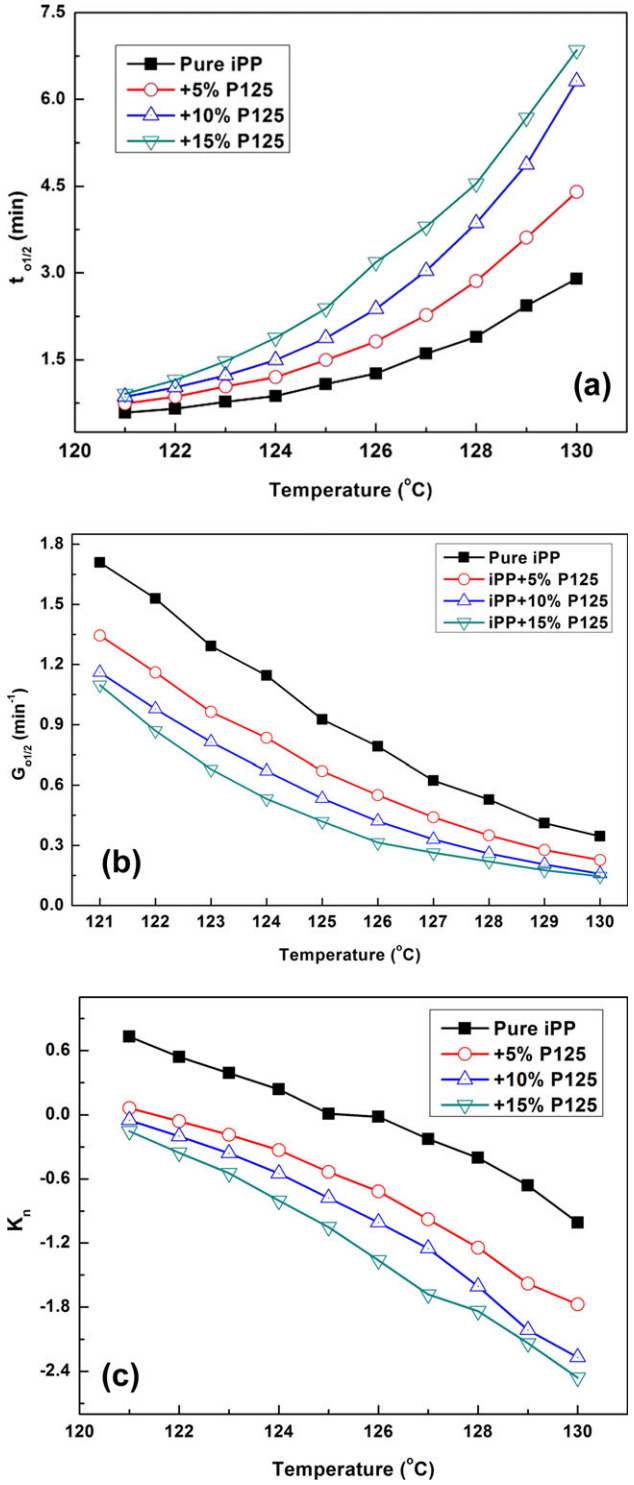


**Figure 7.** Plots of (a) $t_{o1/2}$, (b) $G_{o1/2}$, and (c) $K_n$ as a function of the isothermal $T_c$ of the samples. [Color figure can be viewed in the online issue, which is available at wileyonlinelibrary.com.]

Hoffman and coworkers[49–53] proposed an equation based on the Turnbull and Fisher equation, which is usually referred to as Lauritzen–Hoffman theory [eq. (9)]. For a plain polymer, the equation is as follows:

$$\ln G = \ln G_0 - \left[\frac{u^*}{r(t_c - t_\infty)}\right] - \left[\frac{k_g}{t_c\,\delta t\, f}\right] \tag{9}$$

where $G_0$ is a constant and includes all of the terms that are temperature-insensitive, $U^*$ is the transport activation energy and is equal to 1500 cal/mol, $R$ is the gas constant and is equal to 8.314, $K_g$ is the nucleation parameter, $T_\infty$ is the temperature below which motions cease and is usually taken as $T_\infty = T_g - 30$ K, $\Delta T = T_m^0 - T_c$ is the degree of undercooling in which $T_m^0$ is the equilibrium melting temperature, and $f$ is a factor that accounts for the variation in the enthalpy of fusion ($\Delta h_f$) with temperature, and is obtained by

$$f = 2t_c/\left(t_m^0 + t_c\right)$$

However, the binary blend system in this study contained a crystallizable and an amorphous component; therefore, the expression of the spherulite radial growth rate was different from that of a plain polymer system. For these blends, the previous equation was modified as follows:[3,54–57]

$$\ln G - \ln \varphi_2 = \ln G_0 - \left[\frac{u^*}{r(t_c - t_\infty)}\right] - \left[\frac{k_g}{t_c\,\delta t\, f}\right] + \frac{0.2t_m^0 \ln \varphi_2}{\delta t} \tag{10}$$

where $K_g$ is also expressed as eq. (11)

$$k_g = n_c b_0 \sigma \sigma_e t_m^0 / \delta h_f k \tag{11}$$

where $\phi_2$ is the volume fraction of the crystallizable component and the $n_c$ value depends on the crystallization regime according to Lauritzen–Hoffman theory. In regimes I and III, which occur at low and high undercoolings, respectively, $n_c = 4$. However, in regime II, which occurs at medium undercooling, $n_c = 2$. According to the literature,[58] in this study, $n_c$ was taken to be 2. $\sigma$ and $\sigma_e$ are the lateral and end surface free energies of the growing crystal, respectively. $b_0$ is the molecular thickness, and $k$ is the Boltzmann constant and is equal to $1.38 \times 10^{-23}$ J/K.

$\sigma$ can also be estimated as follows:

$$\sigma = \alpha \Delta h_f \sqrt{a_0 b_0} \tag{12}$$

where $\alpha$ was empirically obtained to be 0.1 and $a_0 b_0$ represents the cross-sectional area of the polymer chain.[59] $\Delta h_f$, $a_0$, and $b_0$ of PP were supposed to be $1.96 \times 10^8$ J/m$^3$, $5.49 \times 10^{-10}$ m, and $6.26 \times 10^{-10}$ m on the basis of the literature.[60] Therefore, a value of = 11.5 erg/cm$^2$ was obtained from eq. (12).

From the plot of $\ln G + \frac{U^*}{R(T_c - T_\infty)}$ against $\frac{1}{T_c \Delta T f}$ the value of $K_g$ was directly calculated from the slope. Therefore, the value of $\sigma_e$ was estimated simply with eqs. (11) and (12). The variations of $t_{c1/2}$ and $G_{c1/2}$ as a function of $T_c$ are shown in Figure 11, and the $K_g$ and $\sigma_e$ values are listed in Table VII.

Figure 11 suggests that once 5% P125 was added to PP, $G$ of PP significantly decreased. As the amount of P125 increased, $G$ decreased gradually, but the decrease rate was relatively low.

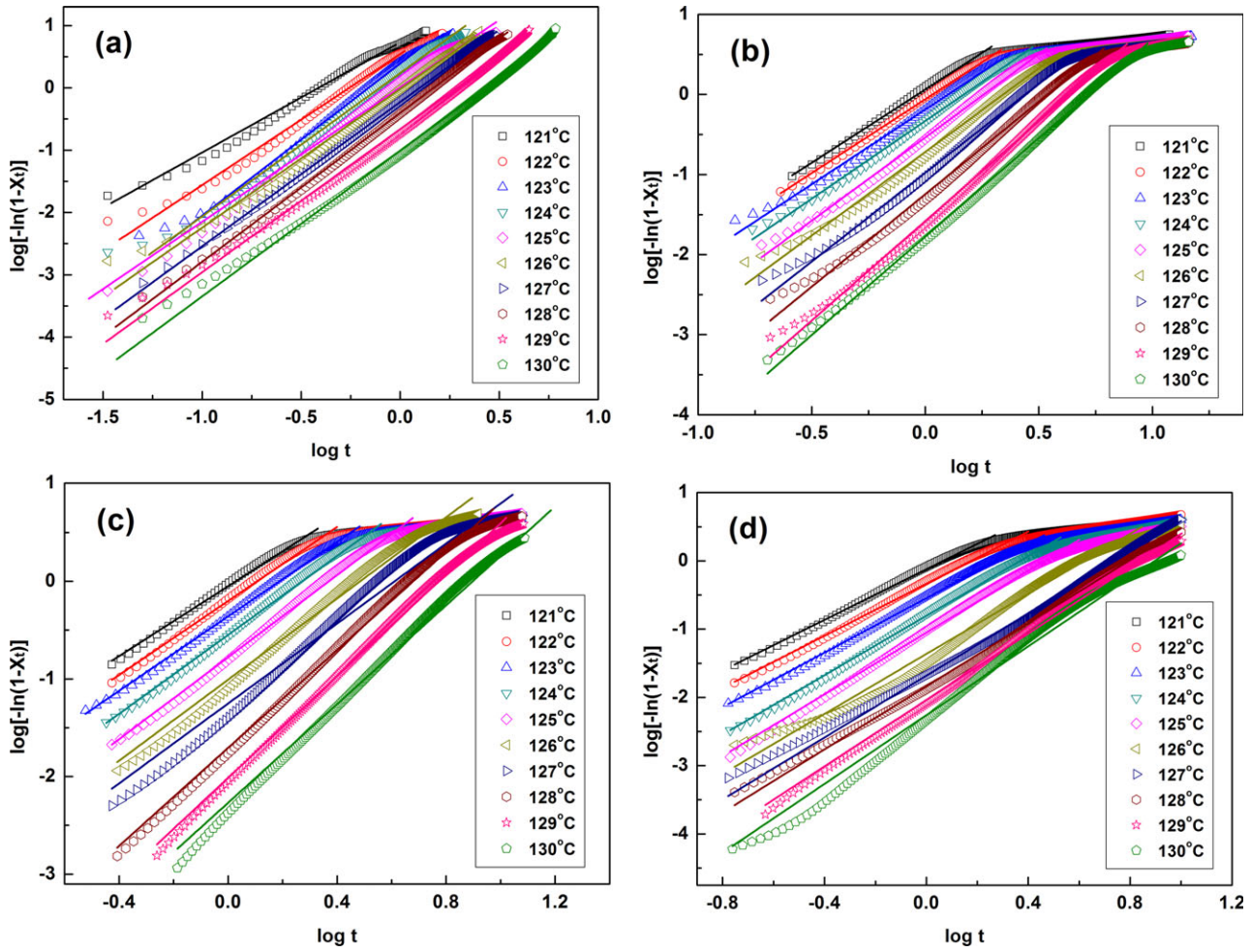


**Figure 8.** Avrami plots of $\log[-\ln(1 - X_t)]$ versus $\log t$ for the isothermal crystallization process for the following samples: (a) pure isotactic polypropylene (iPP), (b) PP + 5% P125, (c) PP + 10% P125, and (d) PP + 15% P125. [Color figure can be viewed in the online issue, which is available at wileyonlinelibrary.com.]

On the other hand, as shown in Table VI, the $K_g$ and $\sigma_e$ values increased gradually as the amount of P125 increased. This indicated that the energy barrier for crystal growth of PP increased, and it became harder for crystal growth to occur. P125 significantly decreased the crystal growth ability of PP.

**Table VI.** *n* Values of the Samples Isothermally Crystallized at 121–130°C

| | Avrami exponent, *n* | | | |
|---|---|---|---|---|
| $T_c$ (°C) | Pure | 5% | 10% | 15% |
| 121 | 1.768 | 1.830 | 1.790 | 1.854 |
| 122 | 2.100 | 1.845 | 1.895 | 1.906 |
| 123 | 2.340 | 1.867 | 1.906 | 1.941 |
| 124 | 2.300 | 1.944 | 1.982 | 1.998 |
| 125 | 2.258 | 2.079 | 2.103 | 2.261 |
| 126 | 2.224 | 2.089 | 2.078 | 2.198 |
| 127 | 2.315 | 2.222 | 2.148 | 2.266 |
| 128 | 2.390 | 2.313 | 2.311 | 2.312 |
| 129 | 2.297 | 2.487 | 2.408 | 2.435 |
| 130 | 2.338 | 2.461 | 2.328 | 2.520 |

### Influence of P125 on the Nucleation Kinetics of PP

As is discussed previously, the results of the isothermal crystallization kinetics show that P125 decreased $G_o$ of PP to a relatively low extent. Meanwhile, the results of the self-nucleation isothermal crystallization kinetics suggest that P125 significantly decreased $G$ of PP. However, the influence of P125 on the nucleation kinetics of PP was still not clear.

In DSC measurement, both the nucleation and crystal growth were shown to make a contribution to $G_o$; this resulted in a mathematical superposition of both bell-shaped curves and the formation of the bell-shaped curve of $G_o$. Therefore, on the basis of the results obtained previously, we plotted the integrated curves of $G_o$ and the growth rate as a function of $T_c$, as shown in Figure 12. The four curves on every sides are $G_o$ (i.e., nucleation and growth rate) and the growth rate parameters obtained, which were only a part of the integrated bell-shaped curves of $G$ or the $G_o$ curves of the samples. The other four curves in the center are the integrated bell-shaped curves we

Applied Polymer SCIENCE

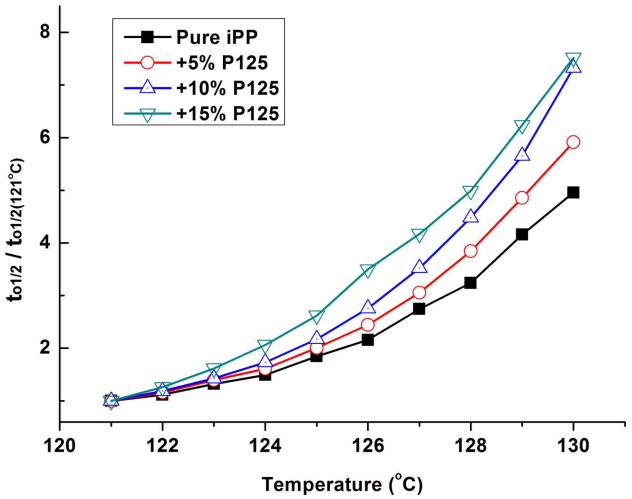


**Figure 9.** Variation trend of $t_{o1/2}$ of the samples with P125 as a function of $T_c$. The $t_{o1/2(121°C)}$ values of the respective samples were taken as references of their own, respectively. [Color figure can be viewed in the online issue, which is available at wileyonlinelibrary.com.]

deduced, where the solid line represents $G_o$ (i.e., the nucleation and growth rate), and the dotted line represents the growth rate only.

Figure 12 shows that for pure PP, the bell-shaped $G_o$ curve was placed in a lower temperature region compared with that of the crystal grow rate only. However, when 5% P125 was added, the $G_o$ curve shifted to a slightly lower $T_c$ value compared with the curve of the pure PP. Meanwhile, the $G$ curve shifted to a lower $T_c$ value significantly and approached the $G_o$ curve. As the amount of P125 increased, the $G_o$ curves shifted to lower $T_c$'s gradually at a low degree, whereas the $G$ curve shifted to lower $T_c$'s to a greater degree. When the amount of P125 was 15%, the $G$ curve was placed at an obviously lower $T_c$ compared with the $G_o$ curve.

Considering that the nucleation and crystal growth contributed to the overall crystallization, we established that the overall crystallization curve should be placed between the nucleation curve and the crystal growth curve. On the other hand, we found in Figure 1 and Table I that P125 decreased $T_c$; this indicated that P125 decreased the nucleation rate of PP. Therefore,

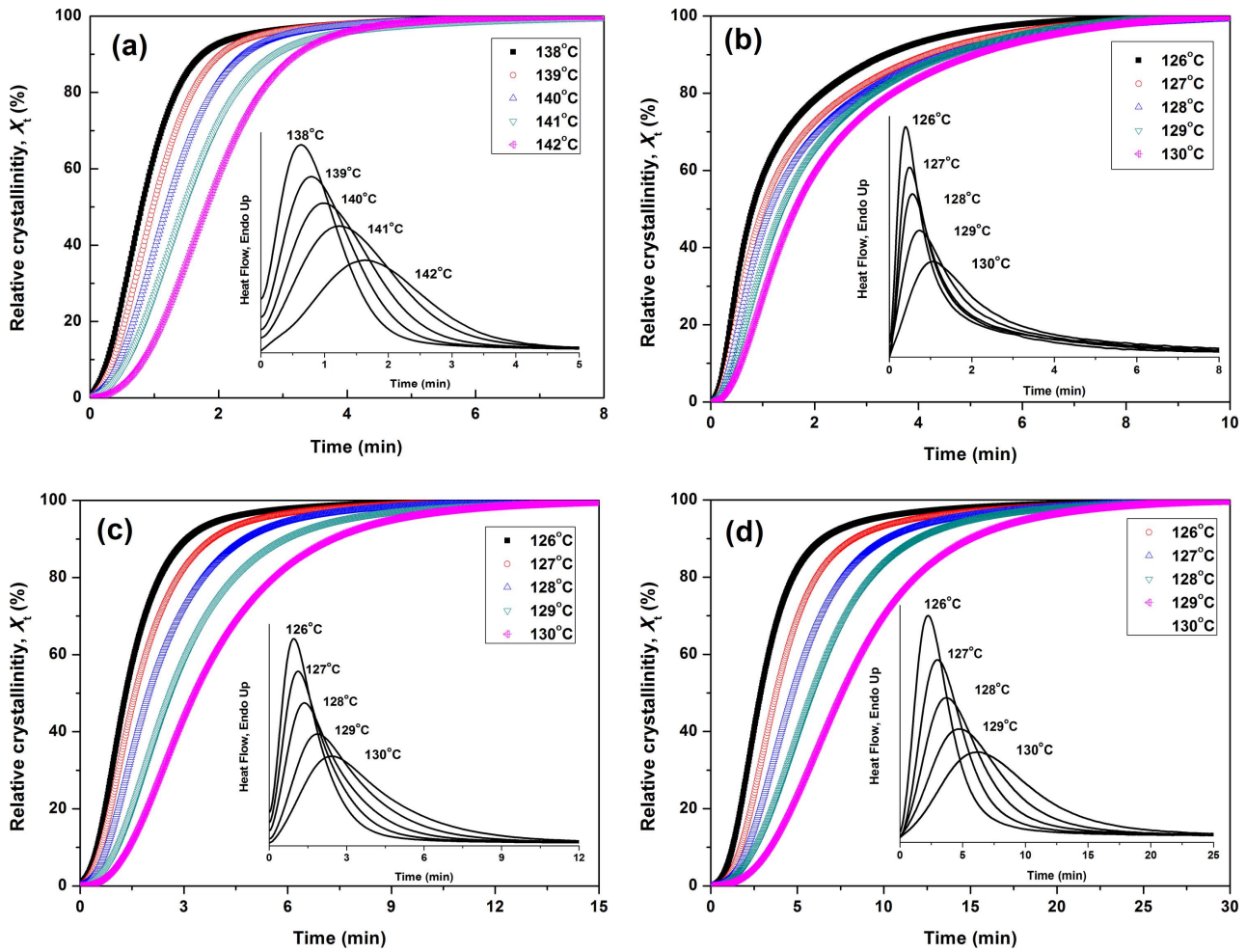


**Figure 10.** Plots of the relative crystallinity versus $t$ for (a) pure PP, (b) 5% P125, (c) 10% P125, and (d) 15% P125 isothermally crystallized after self-nucleation at 167°C. The inset gives the corresponding exothermic DSC curves. [Color figure can be viewed in the online issue, which is available at wileyonlinelibrary.com.]

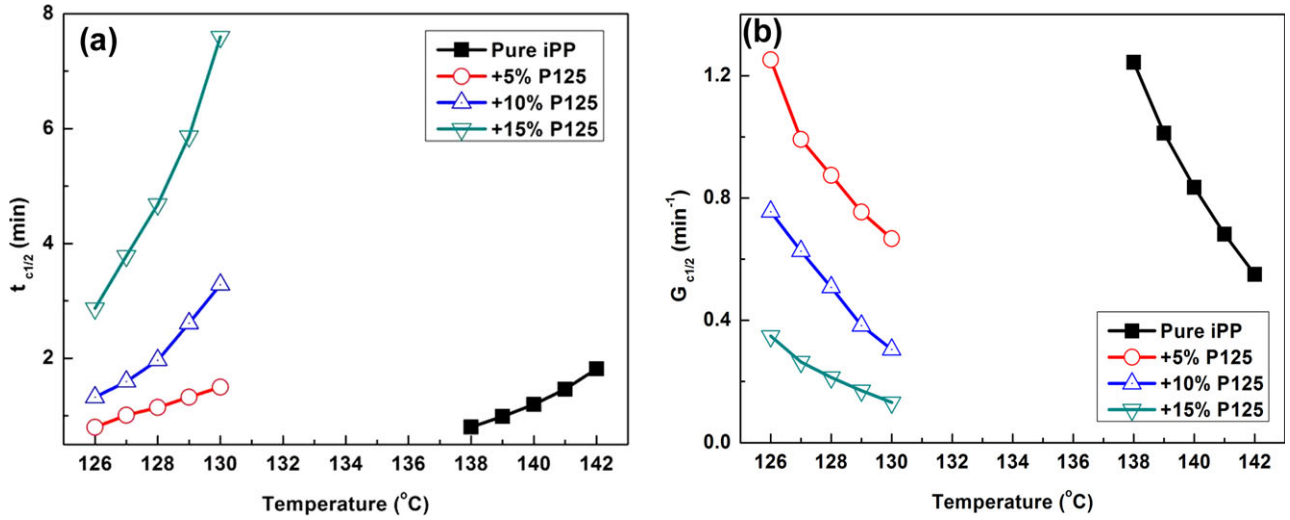


**Figure 11.** (a) $t_{c1/2}$ and (b) $G_{c1/2}$ as a function of the self-nucleation $T_c$ of the samples. [Color figure can be viewed in the online issue, which is available at wileyonlinelibrary.com.]

we deduced that after P125 was added, the bell-shaped nucleation rate curve shifted to lower $T_c$, the decreasing degree of which was lower than that of the overall crystallization curve. When 15% P125 was added, the nucleation rate curve was placed at an obviously higher $T_c$ than that of the $G_o$ curve.

### POM Observation

To directly observe the spherulite morphology of the samples, POM observation was performed. The samples were heated at 200°C for 5 min to erase the thermal history and then cooled down to room temperature at a cooling rate of 5°C/min. After that, the POM micrographs of the samples were taken, as shown Figure 13.

Figure 13 shows that the crystallite morphologies of the samples were quite different from each other. For the pure PP sample, some large spherulites with diameters of about 100 $\mu$m were observed. For PP samples with 5% P125, the spherulites observed were obviously smaller than those of the pure sample, and the number of the spherulites was larger. As the amount of P125 increased (PP with 10 and 15% P125), the sizes of spherulites decreased gradually, and the number of spherulites increased.

These POM results demonstrate that P125 effectively reduced the $L$ values and increased the number of crystallites of PP. From the aspect of crystallization kinetics, this result might have been due to the increase in the nucleation rate or the significant decrease in $G$ during the crystallization procedure. The increase in the nucleation rate should have led to a higher $T_c$; this was, however, not observed in this study. Therefore, the POM results indicated that P125 significantly decreased $G$ of PP and finally reduced $L$; this was consistent with the results of the previous DSC kinetic studies.

### Optical Properties

The crystallization results demonstrated that P125 significantly changed the crystallization behavior and spherulite morphology of PP and might have modified the optical properties of the sample. The optical parameters of the samples, $\tau$, YI, and surface glossiness, were measured and are listed in Table VIII.

As shown in Table VIII, after the addition of P125, $\tau$ decreased, and the surface glossiness increased. This suggested that P125 improved the optical properties of PP. Moreover, the surface glossiness was sensitive to the level of surface flatness;[22] the higher the level of surface flatness was, the higher the surface glossiness of the sample was. The previous results might suggest that P125 increased the surface flatness level of the PP samples. Meanwhile, YI increased when P125 was added; this indicated that the addition of P125 discolored the PP sample. The degree of discoloration increased with increasing amount of P125.

The improvement of $\tau$ in the PP samples after the addition of P125 was attributed to the influence of P125 on the crystallization behavior and crystallite morphology of PP. As we studied, P125 reduced the nucleation rate of PP slightly, decreased the crystal growth significantly, and finally reduced $L$ and the degree of crystallinity. When light propagates through a film, it might be absorbed and scattered by the medium in the film, and most of the contributions of attenuation of light by the film result from scattering by the film. Smaller sizes in the crystallites help to decrease the scattering of light and, finally, help to decrease $\tau$ and improve the transparency of the sample.

**Table VII.** Secondary $K_g$ and $\sigma_e$ Values of the Growing Crystals of the Samples

| Sample | $K_g \times 10^{-4}$ ($K^2$) | $\sigma_e$ (erg/$cm^2$) |
|---|---|---|
| Pure PP | 21.8 | 89.1 |
| +5% P125 | 26.7 | 109.1 |
| +10% P125 | 39.5 | 161.4 |
| +15% P125 | 40.5 | 165.5 |

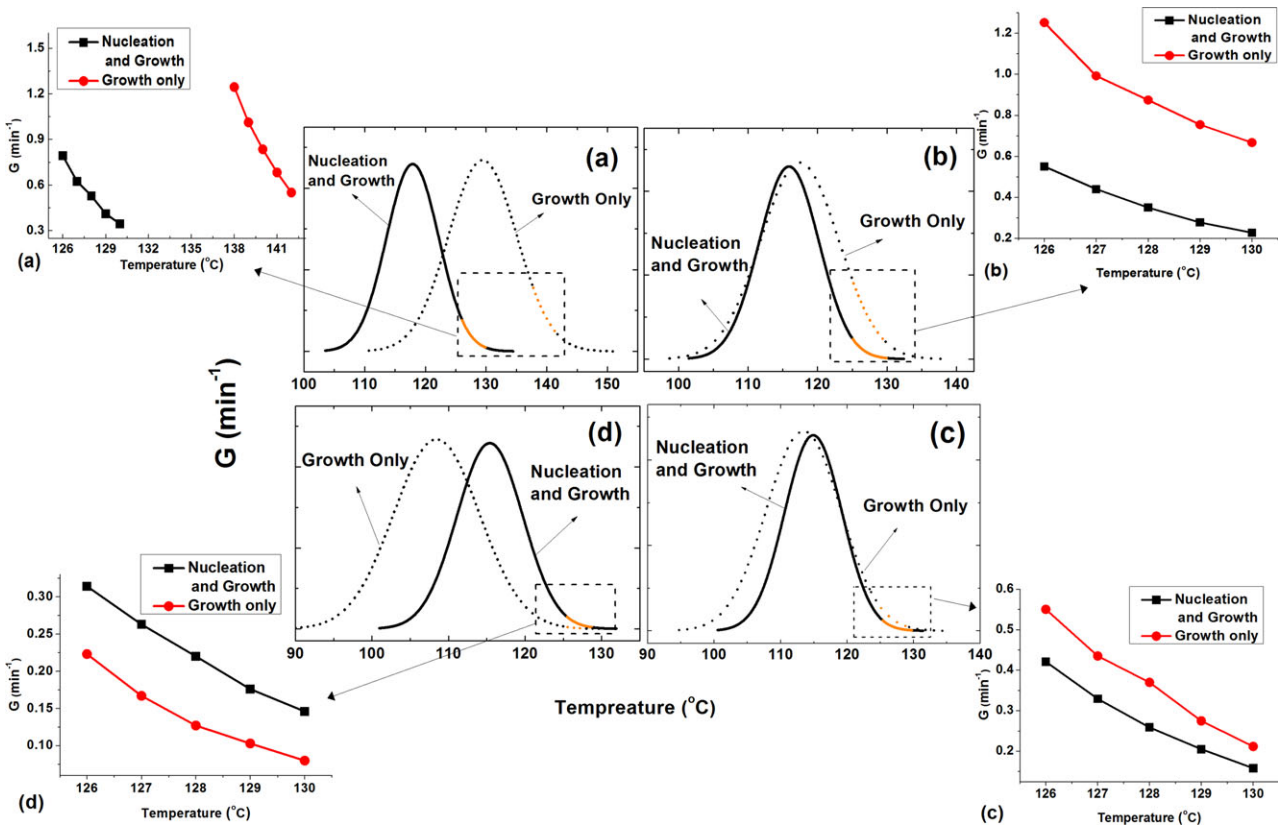


**Figure 12.** Schematic representation of the influence of P125 on the detailed crystallization kinetics of PP. [Color figure can be viewed in the online issue, which is available at wileyonlinelibrary.com.]

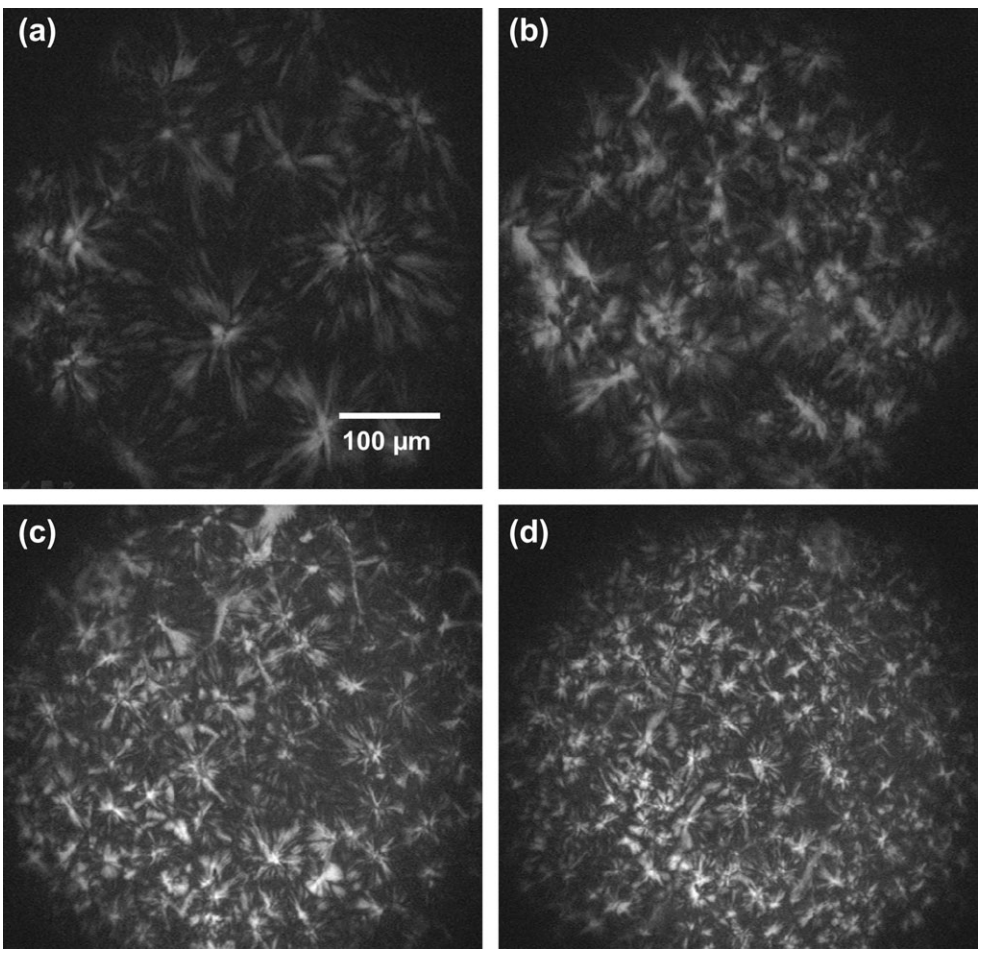


**Figure 13.** Polarized micrographs of spherulites grown during cooling at 5°C/min from the melt (200°C) of the samples.

**Table VIII.** τ, Surface Glossiness, and YI Values of the Samples

| Sample | τ (%) | Surface glossiness (%) | YI |
|---|---|---|---|
| Pure PP | 3.2 | 81.2 | 1.66 |
| +5% P125 | 2.8 | 84.1 | 2.88 |
| +10% P125 | 2.4 | 87.2 | 4.72 |
| +15% P125 | 2.1 | 89.4 | 5.56 |

## CONCLUSIONS

In this study, the influence of the HPR P125 on the crystallization behavior, crystallization kinetics, and optical properties of PP were studied. The conclusions drawn were as follows.

The studies of DSC, SSA, and WAXD demonstrated that P125 reduced the interaction between the PP molecules, decreased the crystallizability of PP, prevented PP from forming thick lamellae, and encouraged the formation thin lamellae.

The investigation of the isothermal crystallization kinetics, self-nucleation isothermal crystallization kinetics, and POM showed that P125 slightly decreased the nucleation rate of PP, significantly decreased $G$, and finally, reduced $G_o$ of PP. The $L$ values of PP were effectively decreased after the addition of P125.

The isothermal crystallization kinetic study over a wide temperature range covering the softening point of P125 demonstrated that the variation rate of $G_o$ under the softening point was obviously lower than that above the softening point; this was attributed to the different phase states of P125 over and below the softening point. Moreover, the dimensionality of crystallization of the PP samples changed after the addition of P125.

The optical properties studies showed that P125 effectively decreased τ and increased the surface glossiness of PP; this was attributed to the influence of P125 on the crystallization behavior and morphology of PP. Meanwhile, P125 increased YI and could discolor the PP sample.

## ACKNOWLEDGMENTS

The authors express their sincere thanks to the Program for New Century Excellent Talents in University (contract grant number NCET-10-0562).

## REFERENCES

1. Cimmino, S.; Di Pace, E.; Karasz, F. E.; Martuscelli, E.; Silvestre, C. *Polymer* **1993**, *34*, 972.
2. Cimmino, S.; Guarrata, P.; Martuscelli, E.; Silvestre, C.; Buzio, P. P. *Polymer* **1991**, *32*, 3299.
3. Di Lorenzo, M. L.; Cimmino, S.; Silvestre, C. *Macromolecules* **2000**, *33*, 3828.
4. Triolo, A.; Silvestre, C.; Cimmino, S.; Martuscelli, E.; Caponetti, E.; Triolo, R. *Polymer* **1998**, *39*, 1697.
5. Cimmino, S.; Duraccio, D.; Silvestre, C. *Macromol. Symp.* **2006**, *234*, 117.
6. Cimmino, S.; Silvestre, C.; Della Vecchia, G. *J. Appl. Polym. Sci.* **2004**, *92*, 3454.
7. Silvestre, C.; Cimmino, S.; Lin, J. S. *J. Polym. Sci. Part B: Polym. Phys.* **2004**, *42*, 3368.
8. Busico, V.; Cipullo, R. *Prog. Polym. Sci.* **2001**, *26*, 443.
9. Kang, J.; Chen, J. Y.; Cao, Y.; Li, H. L. *Polymer* **2010**, *51*, 249.
10. Mandelkern, L. Crystallization of Polymers, 3rd ed.; McGraw-Hill: New York, **2004**.
11. Mark, J. E. Physical Properties of Polymers Handbook; Springer-Verlag: Berlin, German, **2007**.
12. Schultz, J. M. Polymer Crystallization: The Development of Crystalline Order in Thermoplastic Polymers; American Chemical Society: Washington, DC, **2001**.
13. Reiter, G.; Strobl, G. R. Progress in Understanding of Polymer Crystallization; Springer-Verlag, **2007**.
14. Shibayama, M.; Imamura, K. I.; Katoh, K.; Nomura, S. *J. Appl. Polym. Sci.* **1991**, *42*, 1451.
15. Fillon, B.; Wittmann, J.; Lotz, B.; Thierry, A. *J. Polym. Sci. Part B: Polym. Phys.* **1993**, *31*, 1383.
16. Fillon, B.; Lotz, B.; Thierry, A.; Wittmann, J. *Polym. Sci. Part B: Polym. Phys.* **1993**, *31*, 1395.
17. Fillon, B.; Thierry, A.; Wittmann, J.; Lotz, B. *J. Polym. Sci. Part B: Polym. Phys.* **1993**, *31*, 1407.
18. Scherrer, P. *Göttinger Nachrichten* **1998**, *26*, 98.
19. Turner-Jones, A.; Aizlewood, J. M.; Beckett, D. R. *Makromol. Chem.* **1964**, *75*, 134.
20. Pospisil, J.; Habicher, W. D.; Pilar, J.; Nespurek, S.; Kuthan, J.; Piringer, G. O.; Zweifel, H. *Polym. Degrad. Stab.* **2002**, *77*, 531.
21. Klemchuk, P. P.; Horng, P. L. *Polym. Degrad. Stab.* **1991**, *34*, 333.
22. Der Chien, R.; Chen, S. C. *Plast. Rubber Compos.* **2004**, *33*, 155.
23. Kang, J.; Yang, F.; Wu, T.; Li, H. L.; Cao, Y.; Xiang, M. *Eur. Polym. J.* **2012**, *48*, 425.
24. Kang, J.; Yang, F.; Wu, T.; Li, H. L.; Liu, D. M.; Cao, Y.; Xiang, M. J. *Appl. Polym. Sci.* **2012**, *125*, 3076.
25. Muller, A. J.; Arnal, M. L. *Prog. Polym. Sci.* **2005**, *30*, 559.
26. Starck, P. *Polym. Int.* **1996**, *40*, 111.
27. Lehtinen, C.; Starck, P.; Lofgren, B. J. *Polym. Sci. Part A: Polym. Chem.* **1997**, *35*, 307.
28. Muller, A. J.; Hernandez, Z.; Arnal, M. L.; Sanchez, J. *Polym. Bull.* **1997**, *39*, 465.
29. Lorenzo, A. T.; Arnal, M. L.; Mueller, A. J.; Boschetti de Fierro, A.; Abetz, V. *Eur. Polym. J.* **2006**, *42*, 516.
30. Lorenzo, A. T.; Arnal, M. L.; Muller, A. J.; Boschetti-de-Fierro, A.; Abetz, V. *Macromolecules* **2007**, *40*, 5023.
31. Castillo, R. V. N.; Muller, A. J.; Lin, M. C.; Chen, H. L.; Jeng, U. S.; Hillmyer, M. A. *Macromolecules* **2008**, *41*, 6154.
32. Muller, A. J.; Lorenzo, A. T.; Arnal, M. L. *Macromol. Symp.* **2009**, *277*, 207.

33. Lorenzo, A. T.; Arnal, M. L.; Muller, A. J.; Lin, M. C.; Chen, H. L. *Macromol. Chem. Phys.* **2011**, *212*, 2009.
34. Arnal, M. L.; Sanchez, J.; Muller, A. J. *Polymer* **2001**, *42*, 6877.
35. Tanem, B.; Stori, A.; *Polymer* **2001**, *42*, 5389.
36. Virkkunen, V.; Laari, P.; Pitkanen, P.; Sundholm, F. *Polymer* **2004**, *45*, 4623.
37. Virkkunen, V.; Laari, P.; Pitkanen, P.; Sundholm, F. *Polymer* **2004**, *45*, 3091.
38. Trujillo, M.; Arnal, M. L.; Muller, A. J.; Laredo, E.; Bredeau, S.; Bonduel, D.; Dubois, P. *Macromolecules* **2007**, *40*, 6268.
39. Trujillo, M.; Arnal, M. L.; Muller, A. J.; Bredeau, S.; Bonduel, D.; Dubois, P.; Hamley, I. W.; Castelletto, V. *Macromolecules* **2008**, *41*, 2087.
40. Song, S.; Wu, P.; Ye, M.; Feng, J.; Yang, Y. *Polymer* **2008**, *49*, 2964.
41. Gedde, U. W. Polymer Physics; Springer: **1995**.
42. Bond, E. B.; Spruiell, J. E.; Lin, J. S. *J. Polym. Sci. Part B: Polym. Phys.* **1999**, *37*, 3050.
43. Iijima, M.; Strobl, G. *Macromolecules* **2000**, *33*, 5204.
44. Wlochowicz, A.; Eder, M. *Polymer* **1984**, *25*, 1268.
45. Keating, M.; Lee, I. H.; Wong, C. S. *Thermochim. Acta* **1996**, *284*, 47.
46. Avrami, M. *J. Chem. Phys.* **1940**, *8*, 212.
47. Chen, Y. H.; Zhong, G. J.; Lei, J.; Li, Z. M.; Hsiao, B. S. *Macromolecules* **2011**, *44*, 8080.
48. Lorenzo, A. T.; Muller, A. J. *J. Polym. Sci. Part B: Polym. Phys.* **2008**, *46*, 1478.
49. Hoffman, J. D. *Polymer* **1985**, *26*, 803.
50. Hoffman, J. D. *Polymer* **1985**, *26*, 1763.
51. Hoffman, J. D.; Miller, R. L. *Macromolecules* **1989**, *22*, 3502.
52. Hoffman, J. D.; Miller, R. L. *Macromolecules* **1988**, *21*, 3038.
53. Lauritzen, J. J. I.; Hoffman, J. D. *J. Appl. Phys.* **1973**, *44*, 4340.
54. Boon, J.; Azcue, J. M. *J. Polym. Sci. Part A-2: Polym. Phys.* **1968**; *6*, 885.
55. Martuscelli, E. *Polym. Eng. Sci.* **1984**, *24*, 563.
56. Alfonso, G. C.; Russell, T. P. *Macromolecules* **1986**, *19*, 1143.
57. Chen, J. Y.; Cao, Y.; Li, H. L. *J. Appl. Polym. Sci.* **2010**, *116*, 1172.
58. Yang, B. X.; Shi, J. H.; Pramoda, K. P.; Goh, S. H. *Compos. Sci. Technol.* **2008**, *68*, 2490.
59. Feng, Y.; Hay, J. N. *Polymer* **1998**, *39*, 6723.
60. Clark, E. J.; Hoffman, J. D. *Macromolecules* **1984**, *17*, 878.